Concentrated phase emulsion with multicore morphology under shear: A numerical study

A. Tiribocchi,[1,2] A. Montessori,[2] F. Bonaccorso,[1,2,3] M. Lauricella,[2] and S. Succi[1,2,4]

[1]*Center for Life Nano Science@La Sapienza, Istituto Italiano di Tecnologia, 00161 Roma, Italy*

[2]*Istituto per le Applicazioni del Calcolo CNR, via dei Taurini 19, Rome, Italy*

[3]*Department of Physics and INFN, University of Rome Tor Vergata, Via della Ricerca Scientifica 1, 00133 Rome, Italy*

[4]*Institute for Applied Computational Science, John A. Paulson School of Engineering and Applied Sciences, Harvard University, Cambridge, Massachusetts 02138, USA*

(Received 15 June 2020; accepted 4 November 2020; published 30 November 2020)

We numerically study the dynamic behavior under a symmetric shear flow of selected examples of concentrated phase emulsions with multicore morphology confined within a microfluidic channel. A variety of nonequilibrium steady states is reported. Under low shear rates, the emulsion is found to exhibit a solidlike behavior, in which cores display a periodic planetarylike motion with approximately equal angular velocity. At higher shear rates, two steady states emerge, one in which all inner cores align along the flow and become essentially motionless and a further one in which some cores accumulate near the outer interface and produce a dynamical elliptical-shaped ring chain, reminiscent of a treadmillinglike structure, while others occupy the center of the emulsion. A quantitative description in terms of the (i) motion of the cores, (ii) rate of deformation of the emulsion, and (iii) structure of the fluid flow within the channel is also provided.

DOI: 10.1103/PhysRevFluids.5.113606

I. INTRODUCTION

A multiple emulsion is an example of a hierarchical soft fluid, consisting of smaller drops (often named cores) dispersed within a larger one and stabilized by means of surfactants adsorbed onto the interfaces [1–4]. A typical example is a collection of distinct water drops (either monodisperse or polidisperse) encapsulated within an oil one.

Recent microfluidic experiments have been capable of designing highly regular and well-defined multicore emulsions with an extremely controlled procedure [1,3–8]. The process essentially consists of two emulsification steps, one in which water droplets are dispersed in an oil phase and a second one in which they are embedded in the same oil phase [1,3,9]. These results have paved the way to the use of multiple emulsions in a wide range of applications, ranging from pharmaceutics and food science, for delivery and controlled release of compounds [10–12] and for the encapsulation of flavors [13–15], to tissue engineering and cosmetics, for the realization of soft materials with a high degree of porosity [16,17] and for the production of personal care items [2,18].

Understanding the response of these systems to the effect of external fields, even under controlled experimental conditions, remains a crucial requirement for a purposeful design of such emulsion-based devices and for their correct functioning. This is particularly important in concentrated phase emulsions (CPEs) with multicore morphology, in which, unlike the diluted regime, large portions of the material are occupied by fluid interfaces and the volume fraction of the cores is generally higher than 0.3; thus, long-range hydrodynamic interactions as well as droplet collisions cannot be easily neglected [17,19,20]. Indeed an external field, such as a shear flow, can produce relevant interface

deformations that propagate to the scale of the droplet and ultimately compromise the structural integrity and mechanical stability of the whole emulsion.

From a theoretical standpoint, such physics can be almost exclusively investigated by means of numerical simulations built on specific computational models, due to the complicated structure of the equations governing the multiscale dynamics, typically ranging from the size of the interface to that of the microfluidic device [21]. In contrast with the enormous progress achieved in the manufacturing of multiple emulsion [1,3,5,22–25], theoretical studies about their dynamic response under shear have been carried out only more recently (especially for double emulsions [26–29]) and have only partially covered the physics of concentrated phase emulsions [30–32].

It is well known, for example, that when a single-core emulsion is subject to a low or moderate shear flow, the external drop stretches and attains an elliptical shape at the steady state, while the internal core preserves its spherical shape reasonably well [26,28]. Higher shear rates can lead to the breakup of the enveloping shell and the release of the internal drop [33]. When two distinct inner cores are included, an external shear flow can cause the formation of a fluid recirculation, which triggers a periodic planetarylike motion of the cores, lasting over long periods of time within the external droplet [34]. Such features have been captured, with a good level of accuracy, by means of a careful combination of continuum models and numerical simulations, such as boundary integral methods [27] and lattice Boltzmann approaches [29,34]. Yet, much less is known about the dynamics of a multiple emulsion under shear when the number of inner cores augments and their concentration is far from the diluted regime.

In this paper, we go one step further and numerically investigate, by using lattice Boltzmann simulations, the dynamic response of two-dimensional CPEs with multicore morphology in which the area fraction occupied by the cores is higher than 30%. As in previous works [34,35], the physics is described by using a multiphase field model for an immiscible fluid mixture, in which a Landau free energy is employed to calculate the thermodynamic forces (chemical potential and pressure tensor) governing the relaxation dynamics of the system.

By varying the shear rate and number of cores, we provide evidence of nonequilibrium steady states that were previously undetected. At low shear rates, internal cores exhibit a periodic motion, persistent over extended periods of time and triggered by the fluid vorticity. When the number of cores increases, a solidlike dynamic behavior can be envisaged since all cores moves coherently with approximately equal angular speed. At intermediate shear rates, two different steady states are found: one in which cores form a motionless open chain aligned along the flow, and a further one, observed when their number is sufficiently high, in which some aggregate near the external interface and arrange as an elliptical-shaped ring, moving as a treadmill, while others take place in the center of the emulsion and dynamically interact with the former ones. Further increasing the shear rate heavily squeezes the emulsion and forces the cores to arrange in a two-row structure, displaying, once again, a periodic motion along a highly stretched elliptical path. This behavior also leads to significant modifications of the external interface, which, at the steady state, exhibits regular bulges due to the concurrent effect of hydrodynamic interactions and collisions with cores. Such physics is characterized in terms of the (i) motion of the cores (time evolution of center of mass and its velocity), (ii) rate of deformation of the cores, and (iii) structure of the fluid velocity.

The paper is structured as follows. In Sec. II, we describe the computational model and the numerical setup used in the simulations, and in Sec. III, we discuss the results. We start by investigating the response under shear flow of a four-core emulsion, and present some selected nonequilibrium steady states observed at different values of shear rate. Then we report the results about nonequilibrium steady states observed in a higher complex emulsion, in which the number of cores is much increased. Some final remarks conclude the manuscript.

II. THE MODEL

Here we outline the hydrodynamic model of a multicore emulsion, a system made of a collection of immiscible fluid droplets embedded in a larger one. Its physics is captured by the following

coarse-grained fields. A set of scalar phase fields $\phi_i(\mathbf{r}, t)$, $i = 1, \ldots, N$ (where $N + 1$ is the total number of drops and N is the number of cores), represents the droplet density, positive within each drop and zero outside, while the average fluid velocity of both the drops and solvent is described by a vector field $\mathbf{v}(\mathbf{r}, t)$ [34–37].

A. Equations of motion

The dynamics of the fields $\phi_i(\mathbf{r}, t)$ is governed by a set of convection-diffusion equations,

$$\partial_t \phi_i + \mathbf{v} \cdot \nabla \phi_i = M \nabla^2 \frac{\delta \mathcal{F}}{\delta \phi_i}, \tag{1}$$

where M is the mobility and $\mathcal{F} = \int_V f dV$ is the total free energy describing the equilibrium properties of the fluid suspension. A typical expression of the free-energy density f is given by [38,39]

$$f = \frac{a}{4} \sum_i^N \phi_i^2 (\phi_i - \phi_0)^2 + \frac{k}{2} \sum_i^N (\nabla \phi_i)^2 + \epsilon \sum_{i,j,i<j} \phi_i \phi_j, \tag{2}$$

where the first term guarantees the existence of two coexisting minima, $\phi_i = \phi_0$ inside the ith droplet and $\phi_i = 0$ outside, and the second term stabilizes the droplet interface. The parameters a and k are two positive constants controlling the surface tension and width of the interface, which are given by $\sigma = \sqrt{8ak/9}$ and $\xi = 2\sqrt{2k/a}$, respectively [40,41]. Finally, the last term in Eq. (2) is a soft-core repulsion contribution, which penalizes the overlap of droplets and whose strength is gauged by the positive constant ϵ.

The fluid velocity $\mathbf{v}(\mathbf{r}, t)$ obeys the continuity equation (in the incompressible limit)

$$\nabla \cdot \mathbf{v} = 0, \tag{3}$$

and the Navier-Stokes equation

$$\rho \left(\frac{\partial}{\partial t} + \mathbf{v} \cdot \nabla \right) \mathbf{v} = -\nabla p - \sum_i \phi_i \nabla \mu_i + \eta \nabla^2 \mathbf{v}, \tag{4}$$

where ρ is the fluid density, p is its pressure, η is the viscosity of the fluid, and $\mu_i \equiv \frac{\delta \mathcal{F}}{\delta \phi_i}$ is the chemical potential.

B. Numerical details

Equations (1), (3), and (4) are solved by using a hybrid lattice Boltzmann (LB) method, in which the convection-diffusion equations are integrated by using a finite-difference approach, while the continuity and the Navier-Stokes equations are integrated via a standard LB algorithm [42–47].

Multicore emulsions are sandwiched between two parallel flat walls placed at distance L_z (see Fig. 1), where we set neutral wetting for ϕ_i and no-slip conditions for $\mathbf{v}$. The former one is achieved by imposing that $\mathbf{n} \cdot \nabla \mu_i|_{z=0, z=L_z} = 0$ (no mass flux through the walls) and $\nabla(\nabla^2 \phi_i)|_{z=0, z=L_z} = 0$ (interface droplets perpendicular to the walls), where $\mathbf{n}$ is a unit vector normal to the boundaries pointing inward. The latter one means that $v_z(z = 0, z = L_z) = 0$.

In Fig. 1, we show two examples of CPEs, inspired by experiments realized in the laboratory [3,4,23,48] and made of approximately monodisperse cores arranged in a highly symmetric fashion. In Fig. 1(a), four cores (yellow), each of diameter $D_i = 30$ lattice sites, are accommodated within a larger circular region (the second fluid component in black), of diameter $D_O = 100$ lattice sites, in turn surrounded by an external fluid (yellow). Each field ϕ_i is positive and equal to $\simeq 2$ within each core, and zero elsewhere, while the external fluid is positive out of the emulsion, and zero within. In Fig. 1(b), a larger number of cores ($N = 19$), each of diameter $D_i = 20$ lattice sites, is included within a circular drop, of diameter $D_O = 136$ lattice sites, immersed in a further fluid. In both cases,

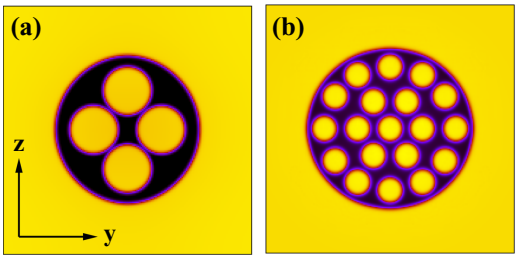

FIG. 1. Equilibrium configurations of (a) a four-core emulsion, $N = 4$, and (b) a 19-core one, $N = 19$. Only a section of the channel is shown. The colors correspond to the values of ϕ, ranging from 0 (black, middle phase) to $\simeq 2$ (yellow, inner and outer phases), while red lines indicate the droplet interface.

the area fraction $A_f = N\pi R_i^2/\pi R_O^2$ occupied by the cores is approximately 0.4, considerably below the close-packing limit ($\sim$0.74), but sufficiently high to be far from the diluted regime and well within the concentrated one [49].

Such emulsions are initially relaxed towards a near-equilibrium state, and afterwards a symmetric shear is applied by moving the top wall along the positive y axis with velocity v_w and the bottom one along the opposite direction with velocity $-v_w$. The resulting shear rate is $\dot{\gamma} = 2v_w/L_z$. In our simulations, v_w ranges between 10^{-2} (low shear) and 4×10^{-2} (moderate and high shear), which means that in a channel of transversal size $L_z = 170$, $\dot{\gamma}$ varies from $\simeq 10^{-4}$ to $\simeq 3.5 \times 10^{-4}$. The dynamic evolution of the emulsion is computed with respect to a dimensionless time $t^* = \dot{\gamma}(t - t_{\rm eq})$, where $t_{\rm eq}$ is the relaxation time after which the shear is imposed, approximately equal to $t_{\rm eq} \simeq 10^5$ time steps [26,28,34]. If not elsewhere stated, the thermodynamic parameters used in our simulations are the following: $a = 0.07$, $M = 0.1$, $\eta = 1.67$, $k = 0.1$, $\epsilon = 0.05$, $\Delta x = 1$, $\Delta t = 1$, where Δx and Δt are the lattice spacing and the integration time step. Dimensions of the lattice are set as follows: $L_y = 400$ and $L_z = 170$ for the four-core emulsion, while $L_y = 800$ and $L_z = 250$ for the 19-core emulsion.

Our system can be approximately mapped onto a multicore emulsion in which internal drops, of diameter $\simeq$10–50 μm and surface tension ranging between 1 and 10 mN/m, are immersed in a fluid of viscosity $\simeq 10^{-1}$ Pa s, assumed equal for both continuous (background fluid) and dispersed (cores) phases [1,35,50]. Typical speeds vary between 0.1 and 0.5 mm/s under a shear rate of 0.1–1/s. Finally, both capillary and Reynolds numbers vary between 0.1 and 5. If, for instance, $v = 0.01$ (in simulation units), one gets $\mathrm{Ca} = \frac{v\eta}{\sigma} \simeq 0.2$ and $\mathrm{Re} = \frac{\rho v D_O}{\eta} \simeq 0.6 - 1.2$, assuming the diameter of the emulsion D_O is a characteristic length, typically ranging from 50 to 100 lattice units.

III. RESULTS

We start by investigating the dynamic response under a symmetric shear flow of the concentrated phase emulsion shown in Fig. 1(a) and afterwards we discuss the case shown in Fig. 1(b).

A. Four-core emulsion

In a previous work [34], we have studied the dynamic behavior of a two-dimensional (2D) multicore emulsion in which two or three cores are dispersed within a larger drop at a relatively low area fraction A_f, ranging from 0.1 to 0.2. We have shown that if the shear rate is kept sufficiently low to avoid the emulsion breakup, at the steady state the cores exhibit a periodic planetarylike motion, caused by a fluid vortex formed within the emulsion and triggered by the sheared structure of the flow. Here we show that such description holds only partially when the area fraction of the cores increases up to 0.4 (like in a concentrated phase emulsion) since significant modifications of both emulsion shape and dynamics occur.

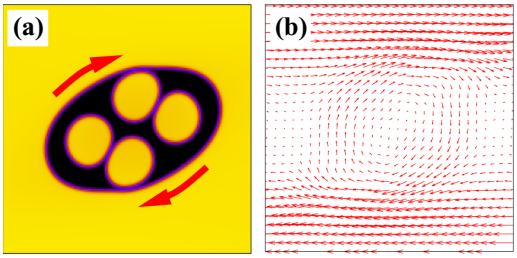

FIG. 2. (a) Typical nonequilibrium steady state of a four-core emulsion under a symmetric shear flow with $\dot{\gamma} \simeq 10^{-4}$ ($v_w = 0.01$). A clockwise rotation of the internal cores is triggered by a fluid recirculation produced by the shear within the emulsion. Red arrows indicate the direction of rotation. (b) Steady-state velocity field under shear. The snapshots are taken at $t^* = 72$. Here, Ca $\simeq 0.2$ and Re $\simeq 1.2$.

In Fig. 2 (and in the Supplemental Material [51], movie M1, where the full dynamics is reported), we show a typical steady-state configuration of a four-core emulsion for $\dot{\gamma} \simeq 10^{-4}$. The motion proceeds essentially as discussed for emulsions with a lower number of cores. Once the shear is imposed, they acquire motion and periodically rotate clockwise in a self-repeating manner around a common center of mass, following approximately circular orbits within the surrounding fluid capsule, which acts as an effective confining bag. The time evolution of their center of mass (Fig. 3) shows that such dynamics is persistent, and no appreciable deviations from it are observed at late time.

As long as the droplet shape remains sufficiently well defined (such as a circle or an ellipse), shape deformations can be reasonably captured by the Taylor parameter $D = \frac{a-b}{a+b}$, where a and b are the length of the major and the minor axis, respectively. In Fig. 4, we show the steady-state time evolution of D of the external droplet and of one of the cores. The former is approximately four times larger than the latter (whose deformation remains negligible), and both exhibit time oscillations due to the reciprocal and recurring interactions among cores and with the external interface. This result proves, once again, that the outer droplet acts as an effective shield, preventing relevant deformations of the inner cores [34].

However, how "long lived" are such steady states? In other words, can the periodic dynamics of the cores turn into an alternative steady configuration before the inevitable rupture?

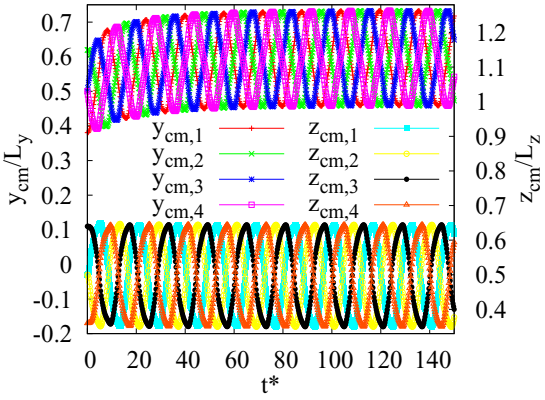

FIG. 3. Time evolution of the y (left axis, top plots) and z (right axis, bottom plots) components of the center of mass of the cores at the steady state. They are computed as $y_{\mathrm{cm},i}(t) = \frac{\sum_y y(t)\phi_i(y,z,t)}{\sum_y \phi_i(y,z,t)}$ and $z_{\mathrm{cm},i}(t) = \frac{\sum_z z(t)\phi_i(y,z,t)}{\sum_z \phi_i(y,z,t)}$, taken where $\phi_i > 0.01$.

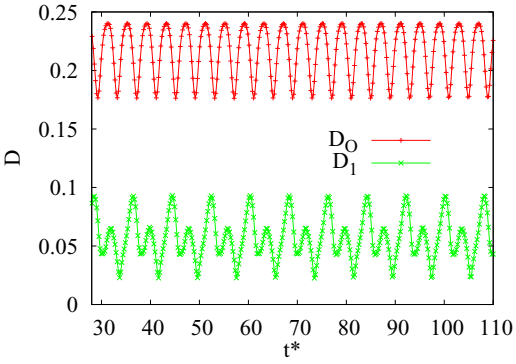

FIG. 4. Time evolution of the Taylor parameter of the outer droplet D_O and of one of the cores, D_1. Time oscillations are due to reciprocal interactions among internal droplets and with the external interface [34].

In Fig. 5 (and the Supplemental Material [51], movie M2), we show, for example, the dynamic evolution of a four-core emulsion for $\dot{\gamma} \simeq 2.4 \times 10^{-4}$. Here, the diffusion constant is $\Gamma = Ma = 3.5 \times 10^{-4}$, with $M = 5 \times 10^{-3}$, and it is lower than the value of the previous case. Note that diminishing Γ, at fixed shear rate $\dot{\gamma}$, increases the Peclet number $\mathrm{Pe} = D_O v_{\max}/\Gamma$, a dimensionless number essentially controlling the mass advection rate with respect to the rate of diffusion. Here, for example, $\mathrm{Pe} \simeq 2850$, while it is $\simeq$140 in Fig. 2. At higher Pe, emulsion deformations are expected to be larger since the mass diffusion rate is considerably lower than the advection rate, despite the system being at moderate values of $\dot{\gamma}$. As long as numerical stability is guaranteed, this ensures that the Reynolds and capillary numbers remain well within the laminar regime, without the need to use very high values of $\dot{\gamma}$.

Like the previous case, once the shear is switched on, the outer droplet tilts along the flow direction and internal cores acquire motion triggered by the fluid vorticity. However, since the flow dramatically increases the eccentricity of the external droplet, such dynamics does not survive at

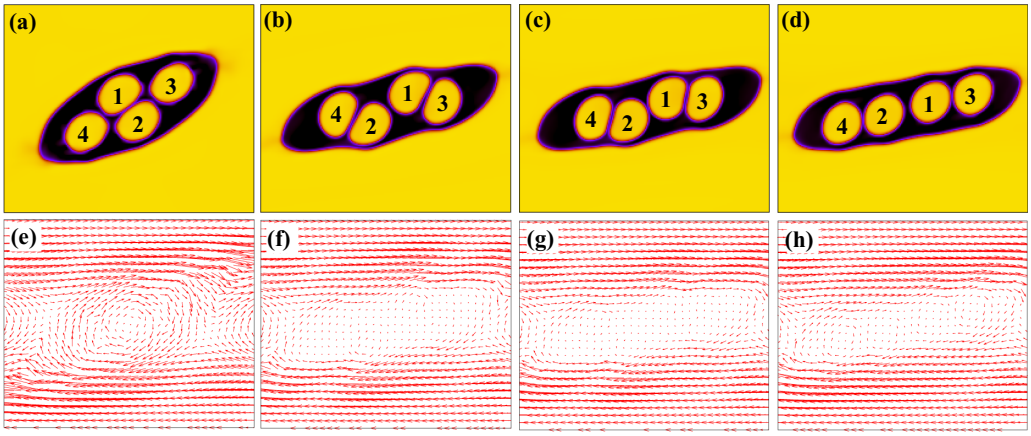

FIG. 5. Top row: Time evolution of a four-core emulsion under a symmetric shear with $\dot{\gamma} \simeq 2.4 \times 10^{-4}$ ($v_w = 0.02$). Cores (a) initially rotate clockwise and, afterwards, (b)–(d) gradually align along the shear flow, due to the large stretching of the external interface which prevents further rotation. Bottom row: Velocity field profile under shear. The internal vortex progressively flattens and the resulting steady-state pattern resembles that of a single fluid under shear. Snapshots are taken at time (a) $t^* = 2$, (b) $t^* = 7$, (c) $t^* = 19$, and (d) $t^* = 31$. Here, $\mathrm{Ca} \simeq 0.4$ and $\mathrm{Re} \simeq 2.4$.

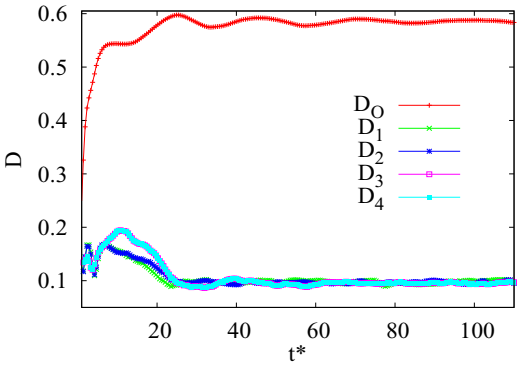

FIG. 6. Time evolution of the Taylor parameter of the outer droplet D_O and of the cores D_1, D_2, D_3, and D_4. The former value is approximately six times higher than the latter ones. Time oscillations at early times progressively weaken and D stabilizes to a roughly constant value.

late times. A large deformation of the outer interface (almost six times higher than that of the cores; see Fig. 6) squeezes the middle fluid and drastically diminishes the mobility of the cores. This effect favors the formation of a quasistationary chainlike aggregate of drops aligned along the shear direction and essentially motionless [see Figs. 5(a)–5(d) and Fig. 7]. The fluid recirculation within

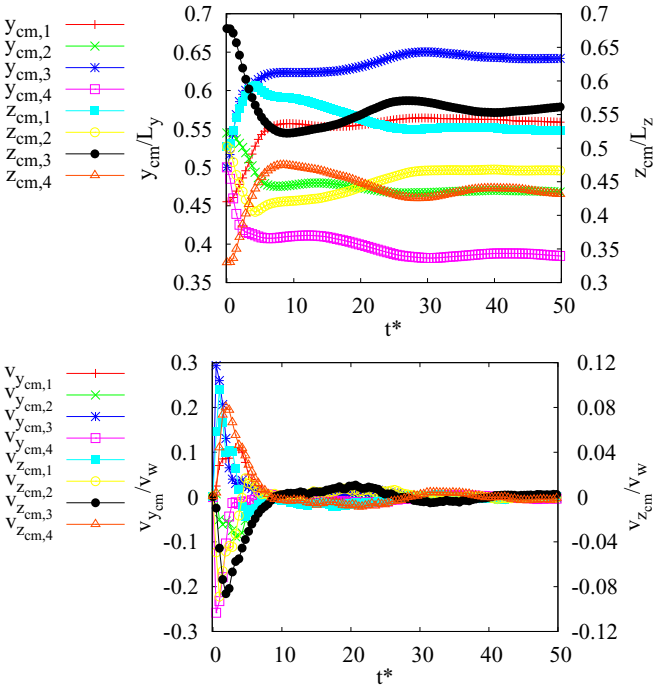

FIG. 7. Top: Time evolution of the y (left axis) and z (right axis) components of the center of mass of the cores. Oscillations progressively flatten at late times since cores stabilize and align along the shear direction. Bottom: Time evolution of the y (left axis) and z (right axis) components of the velocity of the center of mass of the cores. A quick increase of the speed, at early times, is followed by its rapid decay to zero at the steady state.

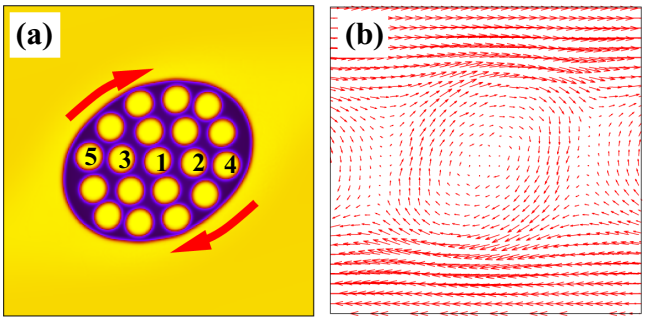

FIG. 8. (a) Typical nonequilibrium steady state of a CPE with 19 cores under a symmetric shear flow with $\dot{\gamma} \simeq 8 \times 10^{-5}$ ($v_w = 0.01$). Once again, a clockwise rotation of the internal cores is triggered by a fluid recirculation produced by the shear within the emulsion. Red arrows indicate the direction of rotation. (b) Steady-state velocity field under shear. Snapshots are taken at $t^* = 11$. Here, Ca $\simeq 0.2$ and Re $\simeq 1.6$.

the emulsion is gradually replaced by an approximately bidirectional flow, reminiscent of the one of a single fluid under shear [see Figs. 5(e)–5(h)], and the speed of each core rapidly decays to zero, after an initial quick increase caused by the sheared structure of the flow in the channel (Fig. 7, bottom). Note, finally, that oscillations of D progressively flatten since collisions among internal cores progressively vanish.

The existence of this further steady state suggests that the dynamic response of a multiple emulsion displays a nontrivial dynamics which, even at low or moderate shear, decisively depends on the number of internal drops as well as on long-range hydrodynamic interactions. In the next section, we investigate the dynamic behavior of a more complex example of a CPE, in which a significantly higher number of cores is included.

B. Higher complex concentrated phase emulsion

Here we discuss the dynamics under a symmetric shear of the concentrated phase emulsion shown in Fig. 1(b), in which 19 cores, each of diameter $D_i = 20$ lattice sites, are included in a larger drop of diameter $D_O = 136$ lattice sites. The area fraction is $A_f \simeq 0.4$. Now, $\dot{\gamma}$ is varied from 8×10^{-5} to 2×10^{-4} ($L_z = 250$), and thus Re ranges from $\sim$1.6 to $\sim$5, and Ca ranges from $\sim$0.2 to $\sim$0.62.

In Fig. 8 (and the Supplemental Material [51], movie M3, for the complete dynamics), we show a typical nonequilibrium steady-state configuration achieved by the 19-core emulsion under shear with $\dot{\gamma} \simeq 8 \times 10^{-5}$. Once again, the cores rotate periodically clockwise due to the internal fluid recirculation, but at a speed depending on the position occupied within the emulsion (see Fig. 9). Indeed, peripheral cores [those near to the external interface, such as 4 and 5 in Fig. 8(a)] follow a quasicircular trajectory larger than the one covered by those [such as cores 1, 2, and 3 in Fig. 8(a)] located close to the center of the emulsion. However, the latter travel at a lower speed and cover a shorter path, employing roughly the same time as the outer cores (Fig. 9). In other words, the whole emulsion behaves as a rigidlike body, in which the angular velocity of the inner and peripheral cores is approximately equal. This is shown in Fig. 10, where the time evolution of the angular speed, computed as $\omega_i(t) = v_{\mathrm{cm},i}(t)/[r_{\mathrm{cm},i}(t) - r_{\mathrm{cm},O}(t)]$, is calculated for two inner and two peripheral cores.

Such periodic dynamics holds as long as the shear rate is kept sufficiently low. Increasing $\dot{\gamma}$ is expected to produce larger shape deformations, potentially yielding to the breakup of the outer droplet and the release of the cores. However, like the lower-core counterparts [34], before such dramatic event, further intermediate nonequilibrium steady states, at low values of Re, can be observed.

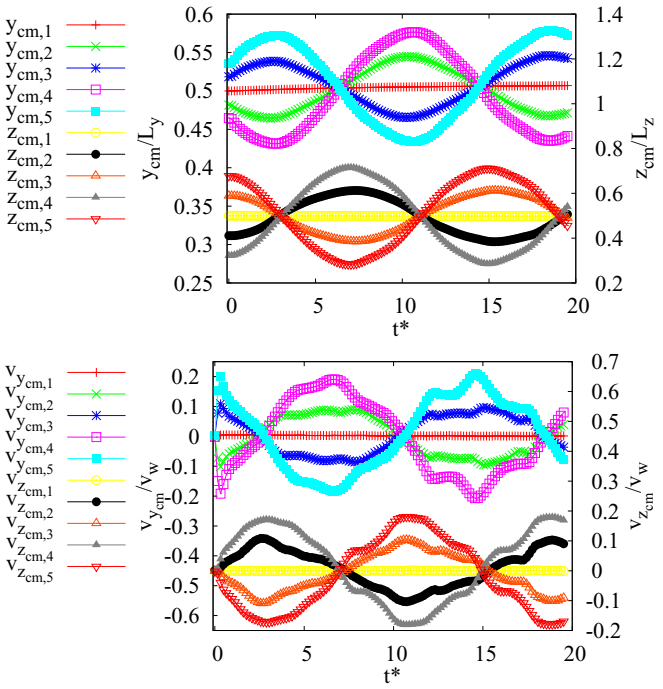

FIG. 9. Top: Time evolution of the y (left axis) and z (right axis) components of the center of mass of five cores (those reported in Fig. 8). All cores follow a periodic dynamics, but the peripheral ones travel along trajectories larger than the ones covered by inner cores. Bottom: Time evolution of the y (left axis) and z (right axis) components of the velocity of the center of mass. Inner cores move at a speed lower than the one of the peripheral cores. The central core is essentially motionless.

In Fig. 11 (and the Supplemental Material [51], movie M4), we show, for example, the dynamic evolution of the emulsion with $\dot{\gamma} \simeq 2.4 \times 10^{-4}$. Clearly, here the shear rate is high enough to produce considerable deformations of the outer droplet, which progressively attains an elliptical-like geometry with a value of D approximately six times higher than that of the cores at the steady state (Fig. 12). The solidlike behavior holds for a short period of time, as long as the emulsion remains approximately circular shaped [Fig. 11(a)]. Afterwards, the external interface stretches

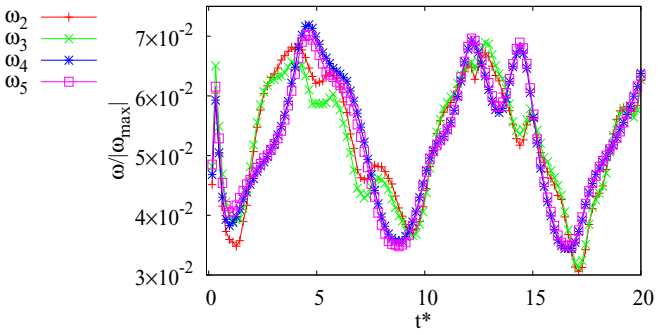

FIG. 10. Typical time evolution of the angular velocity ω of four cores of the emulsion in Fig. 8, calculated with respect to $|\omega_{\max}| \simeq 0.006$. The peripheral and internal cores travel along different paths with approximately equal values of ω.

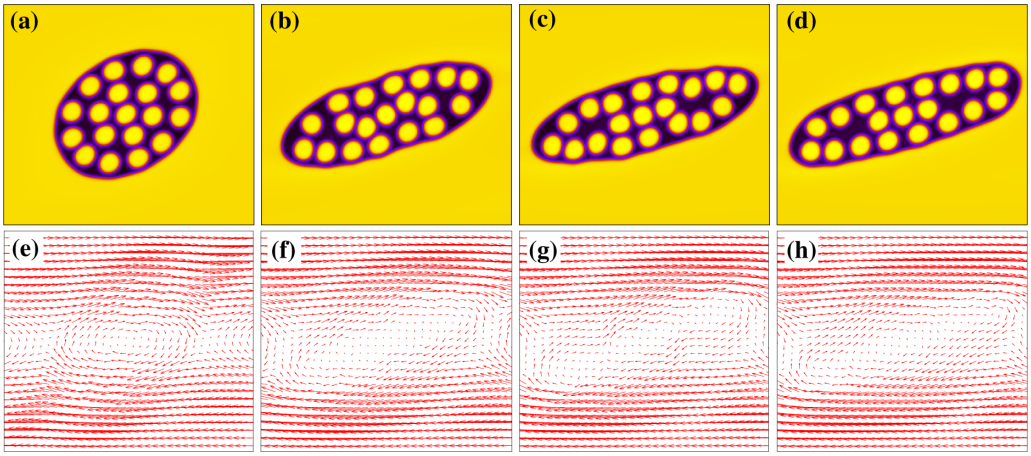

FIG. 11. Top row: Time evolution of a 19-core emulsion under a symmetric shear with $\dot{\gamma} \simeq 2.4 \times 10^{-4}$ ($v_w = 0.03$). The outer droplet preserves its circular shape (a) only for a short period of time since, due to the shear flow, it gradually stretches and attains, at the steady state, (b)–(d) an elliptical-like geometry. (a) While, initially, all internal cores rotate clockwise, (b)–(d) later, some remain in the center of the emulsion and others accumulate close to the outer interface and rotate clockwise. Bottom row: Velocity field profile under shear. Like in Fig. 5, the internal vortex progressively flattens, although, at the steady state, its structure exhibits weak deviations from a plain elliptical pattern due to the motion of the internal cores which perturb the field. Snapshots are taken at time (a) $t^* = 1$, (b) $t^* = 8$, (c) $t^* = 13$, and (d) $t^* = 34$. Here, Ca $\simeq 0.6$ and Re $\simeq 5$.

along the shear flow and the cores, dragged by the fluid current, gradually rearrange. In particular, the peripheral ones accumulate close to the interface and form a dynamic ring chain rotating periodically along elliptical trajectories. On the other hand, the ones located in the middle of the emulsion only temporarily align along the shear direction [Figs. 11(b) and 13]. Later on, some fill the "voids" occasionally left within the chain and get in line, and others remain in the middle of the emulsion due to the lack of space and are recursively hit by the surrounding drops. At the steady state, the peripheral drops exhibit a periodic dynamics reminiscent of a treadmillinglike motion, while the central ones display weak but regular perturbations caused by the interactions with the

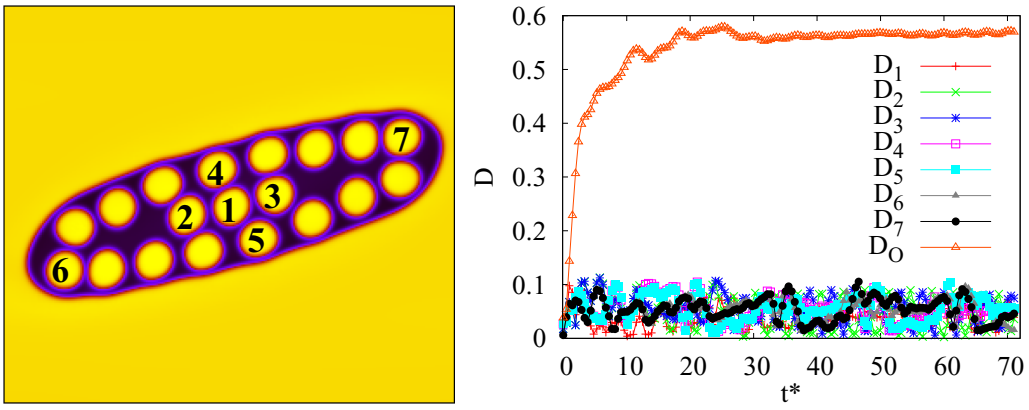

FIG. 12. Left: Typical steady-state configuration of the multicore emulsion taken at $t^* = 34$. Right: Time evolution of the deformation parameter D of the outer droplet (D_O) and of the cores (from D_1 to D_7). At the steady state, the former is roughly six times higher than the latter.

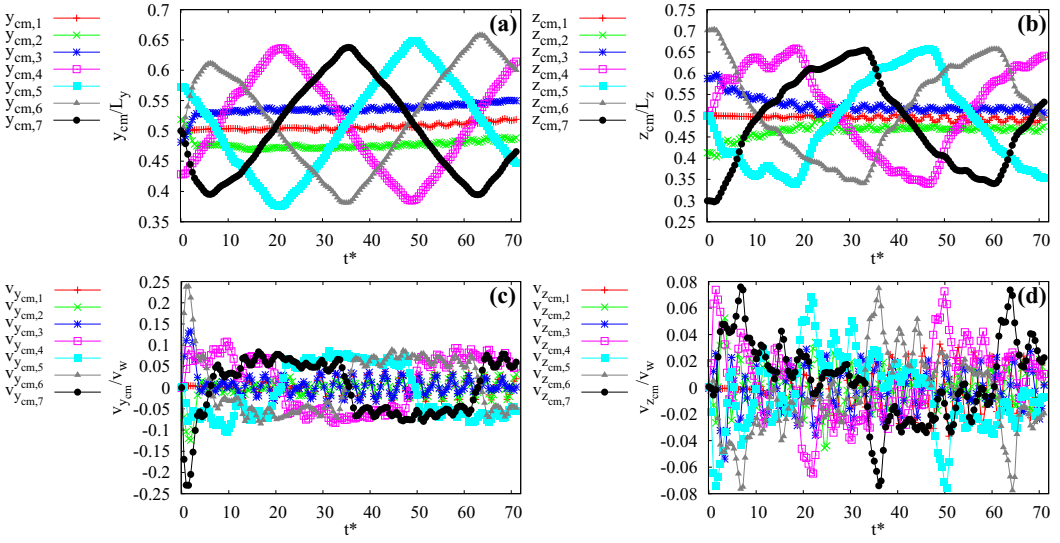

FIG. 13. Top: Time evolution of the (a) y and (b) z components of the center of mass of the cores numbered in Fig. 12. Bottom: Time evolution of the (c) y and (d) z components of their center-of-mass velocity. At the steady state, three cores very weakly fluctuate in the middle of the emulsion, while the others rotate periodically clockwise, with $v_{y_{cm}}$ twice as large as $v_{z_{cm}}$.

remaining cores. Finally, unlike the low shear rate case, here the speed of the cores shows irregular and short peaks, a further signature of the recurring interactions among drops and with the external interface.

C. Shapes and dynamic regimes

The nonequilibrium states described so far have provided two typical examples of configurations attained by the emulsion under low and moderate values of $\dot{\gamma}$. A more detailed overview of the shapes and dynamic regimes observed by varying $\dot{\gamma}$ is reported in Fig. 14.

As mentioned above, the solidlike behavior described in Fig. 8 holds as long as $\dot{\gamma}$ is approximately equal to 1.2×10^{-4} [Fig. 14(a)]. For $1.3 \times 10^{-4} \leqslant \dot{\gamma} \leqslant 1.5 \times 10^{-4}$, the central drop,

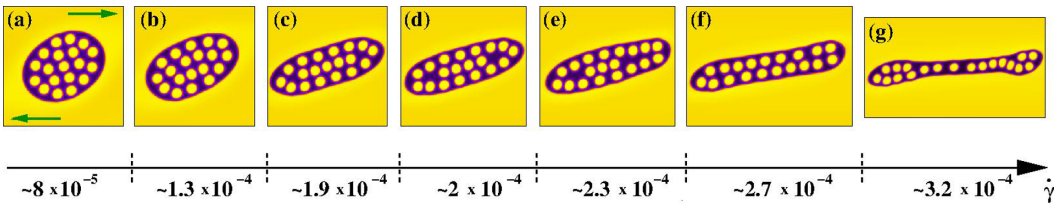

FIG. 14. Approximate nonequilibrium steady states of a 19-core emulsion attained for different values of $\dot{\gamma}$. Green arrows indicate the direction of the moving walls. This applies to all snapshots. For increasing values of the shear rate, the shape of the emulsion varies from (a) a weakly eccentric ellipse towards (b)–(d) a mild and (e),(f) a highly stretched one, up to (g) a state characterized by two bulges connected by a thinner layer of fluid. The cores generally move along elliptical trajectories, but, at (c)–(e) high values of shear rates, some accumulate in the middle of the emulsion where they are repeatedly hit by those in the surroundings. At very high $\dot{\gamma}$, the regular circular motion is replaced by (g) a more chaotic one, in which some cores aggregate and rotate within the bulges of the stretched droplet, while others fluctuate in the connecting layer of fluid.

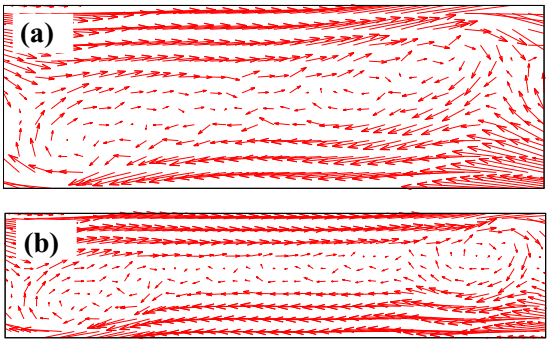

FIG. 15. Velocity profiles observed within and in the surrounding of the emulsions shown in Figs. 14(f) and 14(g). The highly stretched recirculation structure shown in (a) is replaced, in (b), by two separate clockwise vortices located at the extremities of the emulsion and connected by a thin layer of fluid where a weaker and irregular fluid pattern is found.

previously at rest, is set in motion due to the many-body collisions with the surrounding cores, and the emulsion finally attains a nonequilibrium state in which all drops periodically travel clockwise along two different elliptical trajectories [Fig. 14(b)]. For intermediate values of $\dot{\gamma}$ [ranging from $\sim 2 \times 10^{-4}$ to $\sim 2.5 \times 10^{-4}$; see Figs. 14(c)–14(e)], the shear flow further stretches the emulsion which, at late times, exhibits a dynamic behavior similar to the one described in Fig. 11. Basically, some cores periodically rotate and remain in the vicinity of the external interface, while others align in a row in the middle of the emulsion and, as $\dot{\gamma}$ increases, join the former. This occurs since higher values of the shear rate favor the elongation of the emulsion, thus augmenting the distance among peripheral cores as well as collisions against middle-line drops, which are pushed towards the external interface and orbit accordingly.

At high values of $\dot{\gamma}$ (larger than $\sim 2.5 \times 10^{-4}$, with Re $\sim$ 5.5 and Ca $\sim$ 0.7), the emulsion attains a tank-treading-like configuration [Fig. 14(f)], triggered by a highly stretched fluid recirculation pattern as a consequence of the sheared structure of the fluid [see Fig. 15(a) and the Supplemental Material [51], movie M5, showing the full dynamic behavior]. Here, the heavy elongation of the emulsion forces a two-row arrangement of the cores which move, once again, clockwise but along a highly eccentric elliptical trajectory.

The regular dynamics described so far is finally lost by further increasing $\dot{\gamma}$, a regime where inertial effects become relevant. A possible nonequilibrium state attained at late times is that reported in Fig. 14(g), where the emulsion has undergone a dramatic extension due to the heavy flow (here, Re $\sim$ 6.5 and Ca $\sim$ 0.85; see the Supplemental Material [51], movie M6). A thin layer of fluid links two separate round-shaped bulges located at the extremities [Fig. 15(b)], in which cores are found to rotate due to the fluid vortices in a periodic manner, despite the numerous collisions. Occasionally, they are pushed towards the connecting layer where they either weakly fluctuate due to the irregular structure of the velocity field or are sporadically recaptured within the bulges.

These results suggest that the dynamic response of a multicore emulsion under shear may range among four scenarios. At low shear rate, the emulsion approximately behaves in a solidlike manner since cores move by periodic circular motion at equal angular speed. For intermediate values of $\dot{\gamma}$, some cores form a dynamic ring chain rotating close to the external interface and others, essentially motionless, align, side by side, along the shear flow. At higher values of shear rate, all cores are found to exhibit a treadmillinglike motion occurring along a heavily stretched elliptical trajectory, while, for further increasing values of $\dot{\gamma}$, the regular dynamics generally sustained by fluid vortices is replaced by a combination of circular motion and weak fluctuations, observed within far apart rounded bulges connected by a layer of fluid.

IV. CONCLUSIONS

In conclusion, we have numerically studied the dynamics of a 2D concentrated emulsion with multicore morphology under a symmetric shear flow in the low or mild Reynolds-number regime. Although the shear rate is kept at low or moderate values to avoid the breakup of the emulsion, significant shape deformations occur and different nonequilibrium steady states, previously undetected, are observed. Their formation depends on the number of cores and long-range hydrodynamic interactions, controlled by shear rate and mass diffusivity.

We have considered two examples of concentrated phase emulsions whose design is inspired by compound droplets experimentally realized in microfluidic channels. We observe that under low values of shear rates, the external droplet weakly stretches and attains an elliptical shape aligned along the flow, while the internal ones acquire motion and rotate periodically and in a coordinated manner around a common center of mass. In higher complex multicore emulsions, this effect highlights a solidlike behavior of the system since all cores travel with equal angular speed. At higher shear rates, the external droplet generally undergoes larger deformations, which squeeze the middle fluid and significantly affect the motion of the internal drops. In a low-core emulsion, the latter have been observed to align along the flow and become essentially motionless, while in high-core systems, a more complex dynamics occurs. Some cores form a dynamic ring chain and accumulate near the outer interface where local bulges are produced, while others occupy the center of the emulsion and are recursively hit by the former ones.

Our analysis shows that the dynamics of concentrated phase emulsions with multicore morphology is significantly more complex than the one observed in more diluted systems, due to nontrivial coupling between the fluid velocity and deformations of the fluid interfaces. We hope that our results prove useful to acquire a deeper understanding of the mechanisms governing the dynamic response of confined droplets within capsules flowing within microchannels, which is of potential interest in the design of soft composite materials built from compound emulsions as well as in drug delivery, where the release of a drug stored within the cores can be significantly affected by viscoelastic properties and the shape of the middle fluid [1,52].

ACKNOWLEDGMENTS

A.T., A.M., F.B., M.L., and S.S. acknowledge funding from the European Research Council under the European Union's Horizon 2020 Framework Programme (Grant No. FP/2014-2020) ERC Grant Agreement No. 739964 (COPMAT). The authors also warmly acknowledge discussions with S. Aime, D. Weitz, M. Bogdan, and J. Guzowski.

[1] A. S. Utada, E. Lorenceau, D. R. Link, P. D. Kaplan, H. A. Stone, and D. A. Weitz, Monodisperse double emulsions generated from a microcapillary device, Science **308**, 537 (2005).

[2] S. Datta, A. Abbaspourrad, E. Amstad, J. Fan, S. Kim, M. Romanowsky, H. Shum, B. Sun, A. Utada, M. Windbergs, S. Zhou, and D. A. Weitz, Double emulsion templated solid microcapsules: Mechanics and controlled release, Adv. Mater. **26**, 2205 (2014).

[3] G. T. Vladisavljević, R. A. Nuumani, and S. A. Nabavi, Microfluidic production of multiple emulsions, Micromachines **8**, 75 (2017).

[4] S. Ding, C. A. Serra, T. F. Vandamme, W. Yu, and N. Anton, Double emulsions prepared by two-step emulsification: History, state of the art and perspective, J. Control. Release **295**, 31 (2019).

[5] L. Y. Chu, A. S. Utada, R. K. Shah, J. W. Kim, and D. A. Weitz, Controllable monodisperse multiple emulsions, Angew. Chem. Int. Ed. **46**, 8970 (2007).

[6] A. R. Abate and D. A. Weitz, High-order multiple emulsions formed in poly(dimethylsiloxane) microfluidics, Small **5**, 2030 (2009).

[7] W. Wang, R. Xie, X. J. Ju, T. Luo, L. Liu, and D. A. Weit, Controllable microfluidic production of multicomponent multiple emulsions, Lab Chip **11**, 1587 (2011).
[8] P. S. Cless, J. W. Tavacoli, and P. J. Wilde, One-step production of multiple emulsions: Microfluidic, polymerstabilized and particle-stabilized approaches, Soft Matter **12**, 998 (2016).
[9] T. Y. Lee, T. M. Choi, T. S. Shim, R. A Frijns, and S. H. Kim, Microfluidic production of multiple emulsions and functional microcapsules, Lab Chip **16**, 3415 (2016).
[10] K. Pays, J. Giermanska-Kahn, B. Pouligny, J. Bibette, and F. Leal-Calderon, Double emulsions: How does release occur? J. Control. Release **79**, 193 (2002).
[11] E. C. Sela, M. Chorny, N. Koroukhov, H. D. Danenberg, and G. Golomb, A new double emulsion solvent diffusion technique for encapsulating hydrophilic molecules in PLGA nanoparticles, J. Control. Release **133**, 90 (2009).
[12] R. L. McCall and R. W. Siriami, PLGA nanoparticles formed by single- or double-emulsion with vitamin e-tpgs, J. Vis. Expt. **82**, e51015 (2013).
[13] A. Benichou, A. Aserin, and N. Garti, Double emulsions stabilized by new molecular recognition hybrids of natural polymers, Polym. Adv. Technol. **13**, 1019 (2002).
[14] D. J. McClements, Advances in fabrication of emulsions with enhanced functionality using structural design principles, Curr. Opin. Colloid. Interface Sci. **17**, 235 (2012).
[15] G. Muschiolik and E. Dickinson, Double emulsions relevant to food systems: Preparation, stability, and applications, Compr. Rev. Food Sci. Food Saf. **16**, 532 (2017).
[16] B. G. Chung, K. H. Lee, A. Khadamhosseini, and S. H. Lee, Microfluidic fabrication of microengineered hydrogels and their application in tissue engineering, Lab Chip **12**, 45 (2012).
[17] M. Costantini, C. Colosi, J. Guzowski, A. Barbetta, J. Jaroszewicz, W. Swieszkowski, M. Dentinia, and P. Garstecki, Highly ordered and tunable polyhipes by using microfluidics, J. Mater. Chem. **2**, 2290 (2014).
[18] J. S. Lee, J. W. Kim, S. H. Han, I. S. Chang, H. H. Kang, O. S. Lee, S. G. Oh, and Suhm K. D., The stabilization of l-ascorbic acid in aqueous solution and water-in-oil-in-water double emulsion by controlling pH and electrolyte concentration, Intl. J. Cosmet. Sci. **26**, 217 (2004).
[19] J. P. Raven and P. Marmottant, Microfluidic Crystals: Dynamic Interplay Between Rearrangement Waves and Flow, Phys. Rev. Lett. **102**, 084501 (2009).
[20] A. Montessori, M. Lauricella, A. Tiribocchi, and S. Succi, Modeling pattern formation in soft flowing crystals, Phys. Rev. Fluids **4**, 072201(R) (2019).
[21] M. Bernaschi, S. Melchionna, and S. Succi, Mesoscale simulations at the physics-chemistry-biology interface, Rev. Mod. Phys. **91**, 025004 (2019).
[22] P. Garstecki, H. A. Stone, and G. M. Whitesides, Mechanism for Flow-Rate Controlled Breakup in Confined Geometries: A Route to Monodisperse Emulsions, Phys. Rev. Lett. **94**, 164501 (2005).
[23] L. L. A. Adams, T. E. Kodger, S. H. Kim, H. C. Shum, T. Franke, and D. A. Weitz, Single step emulsification for the generation of multi-component double emulsions, Soft Matter **8**, 10719 (2012).
[24] J. Guzowski and P. Garstecki, Droplet Clusters: Exploring the Phase Space of Soft Mesoscale Atoms, Phys. Rev. Lett. **114**, 188302 (2015).
[25] S. Ma, W. T. S. Huck, and S. Balabani, Deformation of double emulsions under conditions of flow cytometry hydrodynamic focusing, Lab Chip. **15**, 4291 (2015).
[26] X. Chen, Y. Liu, and M. Shi, Hydrodynamics of double emulsion droplet in shear flow, Appl. Phys. Lett. **102**, 051609 (2013).
[27] J. Wang, J. Liu, J. Han, and J. Guan, Effects of Complex Internal Structures on Rheology of Multiple Emulsions Particles in 2D from a Boundary Integral Method, Phys. Rev. Lett. **110**, 066001 (2013).
[28] Y. Chen, X. Liu, and Y. Zhao, Deformation dynamics of double emulsion droplet under shear, Appl. Phys. Lett. **106**, 141601 (2015).
[29] N. Wang, C. Semprebon, H. Liu, C. Zhang, and H. Kusumaatmaja, Modelling double emulsion formation in planar flow-focusing microchannels, J. Fluid Mech. **895**, A22 (2020).
[30] R. Par, Rheology of double emulsions, J. Colloid. Interface Sci. **307**, 509 (2007).
[31] R. Pal, Rheology of simple and multiple emulsions, Curr. Opin. Colloid Int. Sci. **16**, 41 (2011).
[32] J. Tao, X. Song, J. Liu, and J. Wang, Microfluidic rheology of the multiple-emulsion globule transiting in a contraction tube through a boundary element method, Chem. Eng. Sci. **97**, 328 (2013).

[33] K. A. Smith, J. M. Ottino, and M. Olvera de la Cruz, Encapsulated Drop Breakup in Shear Flow, Phys. Rev. Lett. **93**, 204501 (2004).
[34] A. Tiribocchi, A. Montessori, S. Aime, M. Milani, M. Lauricella, S. Succi, and D. A. Weitz, Novel nonequilibrium steady state in multiple emulsions, Phys. Fluids **32**, 017102 (2020).
[35] M. Foglino, A. N. Morozov, O. Henrich, and D. Marenduzzo, Flow of Deformable Droplets: Discontinuous Shear Thinning and Velocity Oscillations, Phys. Rev. Lett. **119**, 208002 (2017).
[36] M. Foglino, A. Morozov, and D. Marenduzzo, Rheology and microrheology of deformable droplet suspensions, Soft Matter **14**, 9361 (2018).
[37] R. Mueller, J. M. Yeomans, and A. Doostmohammadi, Emergence of Active Nematic Behavior in Monolayers of Isotropic Cells, Phys. Rev. Lett. **122**, 048004 (2019).
[38] S. R De Groot and P. Mazur, *Non-Equilibrium Thermodynamics* (Dover, New York, 1984).
[39] G. Lebon, D. Jou, and J. Casas-vazques, *Understanding Non-Equilibrium Thermodynamics: Foundations, Applications, Frontiers* (Springer, New York, 2008).
[40] J. S. Rowlinson and B. Widom, *Molecular Theory of Capillarity* (Clarendon, Oxford, 1982).
[41] T. Krüger, H. Kusumaatmaja, A. Kuzmin, O. Shardt, G. Silva, and E. M. Viggen, *The Lattice Boltzmann Method. Principles and Practice* (Springer, New York, 2017).
[42] S. Succi, *The Lattice Boltzmann Equation: For Complex States of Flowing Matter* (Oxford University Press, Oxford, 2018).
[43] R. Benzi, S. Succi, and M. Vergassola, The lattice Boltzmann equation: Theory and applications, Phys. Rep. **222**, 145 (19992).
[44] L. N. Carenza, G. Gonnella, A. Lamura, G. Negro, and A. Tiribocchi, Lattice Boltzmann methods and active fluids, Eur. Phys. J. E. **42**, 81 (2010).
[45] G. Gonnella, A. Lamura, A. Piscitelli, and A. Tiribocchi, Phase separation of binary fluids with dynamic temperature, Phys. Rev. E **82**, 046302 (2010).
[46] A. Tiribocchi, O. Henrich, J. S. Lintuvuori, and D. Marenduzzo, Switching hydrodynamics in liquid crystal devices: A simulation perspective, Soft Matter **10**, 4580 (2014).
[47] A. Montessori, P. Prestininzi, M. La Rocca, and S. Succi, Lattice Boltzmann approach for complex nonequilibrium flows, Phys. Rev. E **92**, 043308 (2015).
[48] S. A. Nabavi, G. T. Vladisavljevic, and V. Manovic, Mechanisms and control of single-step microfluidic generation of multi-core double emulsion droplets, Chem. Eng. J. **322**, 140 (2017).
[49] Y. Zhu, H. Gao, L. Zou, and D. J McClements, A review of the rheological properties of dilute and concentrated food emulsions, J. Text. Stud. **51**, 45 (2019).
[50] S. Guido and V. Preziosi, Droplet deformation under confined poiseuille flow, Adv. Colloid. Interface Sci **161**, 89 (2010).
[51] See Supplemental Material at http://link.aps.org/supplemental/10.1103/PhysRevFluids.5.113606 for further movies.
[52] G. Pontrelli, E. J. Carr, A. Tiribocchi, and S. Succi, Modeling drug delivery from multiple emulsions, Phys. Rev. E **102**, 023114 (2020).